arXiv:hep-ex/9901027v1 18 Jan 1999

High statistics measurement of the underground muon pair separation at Gran Sasso

The MACRO Collaboration

M. Ambrosio[12], R. Antolini[7], C. Aramo[7,n], G. Auriemma[14,a], A. Baldini[13], G. C. Barbarino[12], B. C. Barish[4], G. Battistoni[6,b], R. Bellotti[1], C. Bemporad [13], E. Bernardini [7], P. Bernardini [10], H. Bilokon [6], V. Bisi [16], C. Bloise [6], C. Bower [8], S. Bussino[14], F. Cafagna[1], M. Calicchio[1], D. Campana [12], M. Carboni[6], M. Castellano[1], S. Cecchini[2,c], F. Cei [11,13], V. Chiarella[6], B. C. Choudhary[4], S. Coutu [11,o], G. De Cataldo[1], H. Dekhissi [2,17], C. De Marzo[1], I. De Mitri[9], J. Derkaoui [2,17], M. De Vincenzi[14,e], A. Di Credico [7], O. Erriquez[1], C. Favuzzi[1], C. Forti[6], P. Fusco[1], G. Giacomelli [2], G. Giannini[13,f], N. Giglietto[1], M. Giorgini [2], M. Grassi [13], L. Gray [4,7], A. Grillo [7], F. Guarino [12], C. Gustavino [7], A. Habig [3], K. Hanson [11], R. Heinz [8], Y. Huang[4], E. Iarocci [6,g], E. Katsavounidis[4], I. Katsavounidis[4], E. Kearns [3], H. Kim[4], S. Kyriazopoulou[4], E. Lamanna [14], C. Lane [5], T. Lari [7], D. S. Levin [11], P. Lipari [14], N. P. Longley [4,l], M. J. Longo [11], F. Loparco [7], F. Maaroufi [2,17], G. Mancarella [10], G. Mandrioli [2], S. Manzoor [2,m], A. Margiotta Neri [2], A. Marini [6], D. Martello [10], A. Marzari-Chiesa [16], M. N. Mazziotta[1], C. Mazzotta [10], D. G. Michael[4], S. Mikheyev [4,7,h], L. Miller [8], P. Monacelli [9], T. Montaruli[1], M. Monteno [16], S. Mufson [8], J. Musser [8], D. Nicoló[13,d], C. Orth [3], G. Osteria [12], M. Ouchrif [2,17], O. Palamara [7], V. Patera [6,g], L. Patrizii [2], R. Pazzi [13], C. W. Peck[4], S. Petrera [9], P. Pistilli [14,e], V. Popa [2,i], A. Rainò[1], A. Rastelli[7], J. Reynoldson[7], F. Ronga [6], U. Rubizzo [12], C. Satriano [14,a], L. Satta [6,g], E. Scapparone [7], K. Scholberg [3], A. Sciubba [6,g], P. Serra-Lugaresi [2], M. Severi [14], M. Sioli [2], M. Sitta [16], P. Spinelli[1], M. Spinetti [6], M. Spurio [2], R. Steinberg[5], J. L. Stone [3], L. R. Sulak [3], A. Surdo [10], G. Tarlè[11], V. Togo [2], D. Ugolotti [2], M. Vakili [15], C. W. Walter [3] , and R. Webb [15].

1. Dipartimento di Fisica dell'Università di Bari and INFN, 70126 Bari, Italy

2. Dipartimento di Fisica dell'Università di Bologna and INFN, 40126 Bologna, Italy

3. Physics Department, Boston University, Boston, MA 02215, USA

4. California Institute of Technology, Pasadena, CA 91125, USA

5. Department of Physics, Drexel University, Philadelphia, PA 19104, USA

6. Laboratori Nazionali di Frascati dell'INFN, 00044 Frascati (Roma), Italy

7. Laboratori Nazionali del Gran Sasso dell'INFN, 67010 Assergi (L'Aquila), Italy

8. Depts. of Physics and of Astronomy, Indiana University, Bloomington, IN 47405, USA

9. Dipartimento di Fisica dell'Università dell'Aquila and INFN, 67100 L'Aquila, Italy

10. Dipartimento di Fisica dell'Università di Lecce and INFN, 73100 Lecce, Italy

11. Department of Physics, University of Michigan, Ann Arbor, MI 48109, USA

12. Dipartimento di Fisica dell'Università di Napoli and INFN, 80125 Napoli, Italy

13. Dipartimento di Fisica dell'Università di Pisa and INFN, 56010 Pisa, Italy

14. Dipartimento di Fisica dell'Università di Roma "La Sapienza" and INFN, 00185 Roma, Italy

15. Physics Department, Texas A&M University, College Station, TX 77843, USA

16. Dipartimento di Fisica Sperimentale dell'Università di Torino and INFN, 10125 Torino, Italy

17. L.P.T.P., Faculty of Sciences, University Mohamed I, B.P. 524 Oujda, Morocco

a Also Università della Basilicata, 85100 Potenza, Italy

b Also INFN Milano, 20133 Milano, Italy

c Also Istituto TESRE/CNR, 40129 Bologna, Italy

d Also Scuola Normale Superiore di Pisa, 56010 Pisa, Italy

e Also Dipartimento di Fisica, Università di Roma Tre, Roma, Italy

f Also Università di Trieste and INFN, 34100 Trieste, Italy

g Also Dipartimento di Energetica, Università di Roma, 00185 Roma, Italy

h Also Institute for Nuclear Research, Russian Academy of Science, 117312 Moscow, Russia

i Also Institute for Space Sciences, 76900 Bucharest, Romania

l Swarthmore College, Swarthmore, PA 19081, USA

m RPD, PINSTECH, P.O. Nilore, Islamabad, Pakistan

n Also INFN Catania, 95129 Catania, Italy

o Also Department of Physics, Pennsylvania State University, University Park, PA 16801, USA

Abstract

We present a measurement of the underground decoherence function using multi-muon events observed in the MACRO detector at Gran Sasso at an average depth of 3800 hg/cm ^{2}. Muon pair separations up to 70 m have been measured, corresponding to parent mesons with $P_\perp \leq 1 \div 2$ GeV/c. Improved selection criteria are used to reduce detector effects mainly in the low distance separation region of muon pairs. Special care is given to a new unfolding procedure designed to minimize systematic errors in the numerical algorithm. The accuracy of the measurement is such that the possible contribution of rare processes, such as $\mu^\pm + N \rightarrow \mu^\pm + N + \mu^+ + \mu^-$, can be experimentally studied.

The measured decoherence function is compared with the predictions of the hadronic interaction model of the HEMAS Monte Carlo code. Good agreement is obtained. We interpret this agreement to indicate that no anomalous $P_\perp$ components in soft hadron-Nucleus and Nucleus–Nucleus collisions are required by the MACRO experimental data. Preliminary comparisons with other Monte Carlo codes point out that the uncertainties associated with the hadronic interaction model may be as large as 20%, depending on the energy. MACRO data can be used as a benchmark for future work on the discrimination of shower models in the primary energy region around and below the knee of the spectrum.

I. INTRODUCTION

The knowledge of hadronic interaction processes plays a fundamental role in studies of cosmic rays in the VHE–UHE range (10^{12} eV $\leq E \leq 10^{17}$ eV). In particular, the interpretation of indirect measurements intended to determine the features of primary cosmic rays, such as spectra and composition, depends on the choice of the hadronic interaction model adopted in the description of the atmospheric shower development. For instance, muons

observed by deep underground experiments are the decay products of mesons originating mostly in kinematic regions (high rapidity and high $\sqrt{s}$) not completely covered by existing collider data. The problem is particularly important for nucleus-nucleus interactions for which available data extend only to a few hundreds of GeV in the laboratory frame. It is therefore crucial to find physical observables which are primarily sensitive to the assumed interaction model rather than to the energy spectra and chemical composition of primary cosmic rays.

The shape of the muon lateral distribution is well-suited for this purpose. In particular it allows the study of the transverse structure of hadronic interactions, which is one of the most relevant sources of uncertainties in the models [1]. In fact, different aspects of the interactions contribute to the lateral distribution. We can qualitatively understand this by simple arguments, valid in a first order approximation. Let us consider a single interaction of a primary nucleon of total energy E_0, producing mesons of energy $E^{\pi,K}$ with transverse momentum $P_\perp$, at a slant height H_{prod}, which eventually decay into muons. Calling r the separation of a high energy muon (*i.e.* moving along a straight line) from the shower axis, we have:

$$r \sim \frac{P_\perp}{E^{\pi,K}} H_{prod}. \tag{1.1}$$

In this simplified description we are neglecting the transverse momentum in the parent decay. The previous expression can be written in a more instructive way, considering that at high energy, apart from terms of the order of $(m_T/E_0)^2$, the longitudinal c.m. variable x_F is approximately equal to the laboratory energy fraction:

$$r \sim \frac{P_\perp}{x_F^{\pi,K} E_0} H_{prod} \propto \frac{P_\perp}{x_F^{\pi,K} E_0} \left(\log \sigma_{n-Air}^{inel} + const. \right). \tag{1.2}$$

The assumption of an exponential atmosphere has been used in the last expression. It can be seen how the transverse and longitudinal components of the interaction, as well as

the inclusive and total cross sections, convolve together (with different weights) to yield the lateral separation. The role of $P_\perp$ remains a dominant one in determining the relative separation of the muon component by introducing a loss of collinearity ("decoherence") with respect to the direction of the shower axis.

A qualitative extension to the case of nuclear projectiles can be made within the framework of the superposition model, where each nucleon of the projectile of mass number A is assumed to interact independently with energy E_0/A. Further refinements are needed to account for modifications in the $P_\perp$ and x_F distributions deriving from the nuclear structure of projectile and target, as will be discussed later. A reliable evaluation of the lateral distribution function can be obtained only by Monte Carlo methods.

Deep underground experiments are capable of selecting atmospheric muons in the TeV range produced in the initial stages of the extensive air shower (EAS) development. They can perform a measurement of muon separation which is highly correlated to the lateral distribution. Since the shower axis position is not usually known, the distribution of muon pair separation in multimuon events is studied. Muons associated with the same events, coming in general from different parent and shower generations, are grouped together. Furthermore, a wide range of primary energy is integrated in the same distribution. It is generally assumed, and supported by many simulations, that the shape of this distribution is only slightly affected by the mass composition of primaries [2], thus preserving the sensitivity to the interaction features. As an example, in Fig. 1 we show the dependence of the average pair separation, as detected at the depth of the underground Gran Sasso laboratory, with respect to the $\langle P_\perp \rangle$ of the parent mesons and to their production slant height in the atmosphere. These have been calculated by means of the HEMAS Monte Carlo code [3] for a mixed primary composition [10]. This code employs an interaction model based on the results of the experiments at hadron colliders.

The decoherence function as measured in an underground experiment is also affected by

multiple scattering in the rock and, to some extent, geomagnetic deflection.

For a detector with geometrical acceptance $A(\theta, \phi)$, for zenith and azimuthal angles θ and ϕ, respectively, we define the decoherence function as the distribution of the distance between muon pairs in a bundle:

$$\frac{dN}{dD} = \frac{1}{\Omega T} \int \frac{1}{A(\theta, \phi)} \frac{d^2 N(D, \theta, \phi)}{dD d\Omega} d\Omega, \tag{1.3}$$

where $N(D, \theta, \phi)$ is the number of muon pairs with a separation D in the direction (θ,ϕ), Ω is the total solid angle covered by the apparatus and T is the total exposure time of the experiment. A muon bundle event of multiplicity N_μ will contribute with a number of independent pairs $N = N_\mu(N_\mu - 1)/2$.

In principle, a decoherence study can be performed without a single large area detector, and in early attempts the muon lateral separation was studied via coincidences between two separate movable detectors [4]. The advantage offered by a single large area detector is the ability to study the features inherent in the *same* multi-muon event, such as higher order moments of the decoherence distribution [5].

The large area MACRO detector [6] has horizontal surface area of $\sim$ 1000 m^2 at an average depth of 3800 hg/cm^2 of standard rock ($E_\mu \geq 1.3$ TeV) and is naturally suited for this kind of measurement. An analysis of the muon decoherence has already been performed [7,8,9,10]. The bulk of multiple muon events in MACRO corresponds to a selection of primary energies between a few tens to a few thousands of TeV/nucleon. Hadronic interactions and shower development in the atmosphere were simulated with the previously noted HEMAS code. In particular, a weak dependence on primary mass composition was confirmed for two extreme cases: the "heavy" and "light" composition models [11]. The MACRO analysis was designed to unfold the true muon decoherence function from the measured one by properly considering the geometrical containment and track resolution efficiencies. This procedure permits a direct comparison between measurements performed by

different detectors at the same depth, and, more importantly, whenever new Monte Carlo simulations are available, allows a fast comparison between predictions and data without the need to reproduce all the details of detector response.

The first attempt, obtained while the detector was still under construction, and therefore with a limited size, was presented in [7]. The same analysis, with a larger sample based on the full lower detector, was extended in [8]. With respect to the HEMAS Monte Carlo expectations, these results indicated a possible excess in the observed distribution at large separations. In Ref. [10] we presented the decoherence distribution without the unfolding procedure; the claimed excesses were not confirmed. In order to reach more definitive conclusions, a more careful analysis of the systematics associated with the unfolding procedure was considered necessary. A detailed discussion of this item will be addressed in Section 4.

A more careful discussion of the Monte Carlo simulation is also necessary. The bulk of the muon bundles collected by MACRO are low multiplicity events, coming from parent mesons in the far forward region of UHE interactions, not easily accessible with collider experiments. This requires an extrapolation to the highest energies and rapidity regions, introducing possible systematic uncertainties. For instance, some doubts have been raised [1] concerning the treatment of meson $P_\perp$ in HEMAS. In the HEMAS hadronic interaction code, secondary particle $P_\perp$ depends upon three different contributions:

- $\langle P_\perp \rangle$ increases with energy, as required by collider data in the central region;
- $\langle P_\perp \rangle$ increases in p–Nucleus and Nucleus–Nucleus interactions, relative to that for pp collisions, according to the "Cronin effect" [12];
- $\langle P_\perp \rangle$ varies with x_F, according to the so called "seagull effect" [13].

The sum of these effects yields some doubt about a possible overestimate of $P_\perp$ for energetic secondary particles, an hypothesis recently restated in [14]. It is therefore crucial to perform

a high precision test of the transverse structure of this model, since it affects the calculation of containment probability for multiple muon events and, consequently, the analysis of primary cosmic ray composition [9,10].

In this paper, a new analysis of the unfolded decoherence function is presented, performed with improved methods up to 70 m. The present work enlarges and completes the data analysis presented in [9,10]. Preliminary results of this unfolding procedure [15] showed an improved agreement between experimental data and Monte Carlo predictions.

Particular attention is paid to the small-separation ($D \leq 1$ m) region of the decoherence curve, in which processes such as muon-induced hadron production can produce a background to the high energy muon analysis. At the energies involved in the present analysis ($E_\mu \geq 1$ TeV), moreover, muon-induced muon pair production in the rock overburden could yield an excess of events with small separation, as suggested in [16]. This process is usually neglected in Monte Carlo models commonly adopted for high energy muon transport [3,17,18,19].

Section 2 is devoted to the description of the detector and of data analysis, with a focus on new event selection criteria. In Section 3 the features of the Monte Carlo simulation are presented together with the comparison between experimental and simulated data in the MACRO detector, while Section 4 is dedicated to the unfolding procedure. A comparative discussion of the features of different hadronic interaction models is summarized in Section 5. In Section 6, the problem existing in the first bins of the decoherence distribution is presented in detail, testing new hypotheses on its origin. Conclusions follow in Section 7.

II. DETECTOR DESCRIPTION AND DATA ANALYSIS

The MACRO detector [6], located in hall B of the Gran Sasso Laboratory, is a large area detector equipped with streamer tube chambers, liquid scintillation counters and nuclear

track detectors arranged in a modular structure of six "supermodules". Each of these is 12 m×12 m×9 m in size and consists of a 4.8 m high lower level and a 4.2 m upper "attico". In this paper only data from the lower level of the apparatus are included; therefore only the lower detector will be described further.

Tracking is performed by means of limited streamer tubes, which are distributed in ten horizontal planes separated by ~ 60 g cm^{-2} of $CaCO_3$ (limestone rock) absorber, and in six planes along each vertical wall. The streamer tubes have a square cross section of 3×3 cm^2, and are 12 m long. From each plane two coordinates are provided, the wire (perpendicular to the long detector dimension) and strip views. The latter employs 3 cm wide aluminum strips at 26.5° to the wire view. The average efficiencies of the streamer tube and strip systems were 94.9% and 88.2% respectively, in the period of this analysis.

The spatial resolution achieved with this configuration depends on the granularity of the projective views. The average width of a cluster, defined as a group of contiguous muon "hits," is 4.5 cm and 8.96 cm for the wire and strip views, respectively. Muon track recognition is performed by an algorithm which requires a minimum number of aligned clusters (usually 4) through which a straight line is fit. The differences between the cluster centers and the fit determine a spatial resolution of σ_W=1.1 cm for the wire view and σ_S=1.6 cm for the strip view. These resolutions correspond to an intrinsic angular resolution of 0.2^0 for tracks crossing ten horizontal planes.

In reconstructing the best bundle configuration, the tracking package flags track pairs as parallel, overlapping, or independent and not parallel. This is achieved in two steps, in each projective view:

- two tracks are defined as parallel if their slopes coincide within 2 σ or if their angular separation is less than 3^0 (6^0 if the tracks contain clusters whose widths exceed 30 cm). Otherwise, the track pair is flagged as independent and not parallel if its distance

separation is larger than 100 cm.

- tracks at short relative distance are labelled as overlapping if their intercepts with the detector bottom level coincide within 3.2 σ (2 σ if their angular separation is $< 1.5^0$).

The routine chooses the most likely bundle as the set having the largest number of parallel tracks and the largest number of points per track. Subsequently, tracks flagged as not parallel are considered in order to include fake muon tracks originated primarily by hadrons or δ-rays in the surrounding rock or inside the detector. A two-track separation of the order of 5 cm is achieved on each projective view. However, this capability can be substantially worsened in case of very large, but rare, catastrophic energy losses of muons in the detector.

Only tracks with a unique association in the two views can be reconstructed in three dimensional space. At this level, pattern recognition is used to require a complete matching between tracks belonging to different projective views. This is automatically achieved when two tracks pass through separate detector modules. When they are in the same module, matching of hit wires and strips on the same detector plane is accomplished by taking advantage of the stereo angle of the strips with respect to the wires. In some cases the track pattern correspondence between the two views is also used. The possibility to analyse muon decoherence in three dimensional space is important to have an unbiased decoherence distribution. However, the unambiguous association of muon tracks from the two projective views cannot be accomplished for high multiplicity events because, in events characterized by a high muon density, the tracking algorithm is not able to resolve the real muon pattern without ambiguities, especially when tracks are superimposed. In Ref. [9,10] we presented the muon decoherence function in the wire view alone, which allowed the extension of the analysis to higher multiplicities.

We have analyzed about $3.4 \cdot 10^5$ events, corresponding to a 7732 hr live time for the lower part of the apparatus. These events were submitted to the following selection criteria:

1. Zenith angle smaller than 60^0. This choice is dictated by our limited knowledge of the Gran Sasso topographical map for high zenith angles. Moreover, we cannot disregard the atmosphere's curvature for larger zenith angles, which at present our current simulation models do not include.

2. Fewer than 45 streamer tube hits out of track. This selection is designed to eliminate possible misleading track reconstruction in events produced by noise in the streamer tube system and/or electromagnetic interactions in or near the apparatus.

3. Track pairs must survive the parallelism cut. This rejects hadrons from photonuclear interactions close to the detector, as well as tracks reconstructed from electromagnetic interactions which survived the previous cut.

The last cut is not completely efficient in rejecting muon tracks originating from local particle production because the angle between these tracks may fall within the limits imposed by the parallelism cut. These limits cannot be further reduced since the average angular divergence due to multiple muon scattering in the rock overburden is about 1^0 at the MACRO depth. This is a crucial point, since these events could contaminate the decoherence curve in the low separation region and are not present in the simulated data because of the excessive CPU time required to follow individual secondary particles. A similar effect could be produced by single muon tracks with large clusters, which may be reconstructed as a di-muon event by the tracking algorithm.

In order to reduce these effects, a further selection was applied. We computed, for each muon track in the wire view, the ratio R between the number of streamer tube planes hit by the muon to the number of planes expected to be hit considering the track direction. Only tracks with $R \geq 0.75$ were accepted. The application of this cut (hereafter cut C4) in the wire view alone is a good compromise between the rejection capability of the algorithm and the loss of events due to the unavoidable inefficiency of the streamer tube system. We found

that in the wire projective view the probability to reject a muon track due to contiguous, inefficient planes is 2.0%.

To show the effects produced by cut C4, we present in Fig. 2 the fractional differences between the experimental decoherence curve before and after its application. As expected, the new cut affects only the first bins of the distribution.

To test the ability of cut C4 to reject hadronic tracks, we used FLUKA [17] to simulate 3028 hr of live time in which muons were accompanied by hadronic products of photonuclear interactions in the 10 m of rock surrounding the detector. We found that the parallelism cut alone provides a rejection efficiency of about 54.6% of the pair sample, while the addition of cut C4 enhances the rejection to 95.9%. The effect of hadron contamination, furthermore, is very small, contributing less than 1% in the overall muon pair sample. This estimate, together with the plot of Fig. 2 and the results of a visual scan, suggest that the main track sample rejected by cut C4 is made of large cluster tracks. After the overall application of these cuts, the number of surviving unambiguously associated muon pair tracks is 355,795. In Fig. 3 the percentage of the reconstructed events as a function of muon multiplicity is shown (open circles). In the same figure, the percentage of the unambiguously associated muon pairs as a function of the multiplicity is also reported (black circles). Due to detector effects, the number of associated pairs N'_{pair} in an event of multiplicity N_μ is generally smaller than the maximum number of independent pairs $N_{pair} = N_\mu(N_\mu - 1)/2$. This reduction becomes greater for high multiplicities, for obvious reasons of track shadowing. In any case, we still find that the weight of high multiplicity events remains dominant in the decoherence distribution. In order to reduce this effect and to reduce the possible dependence on primary composition, we have assigned a weight $1/N'_{pair}$ to each entry of the separation distribution. This prescription, followed also for simulated data, has been already applied in most of the previous analyses performed by MACRO. Moreover, we emphasize that the focus of this analysis is centered on the shape of the distribution; the absolute rate of pairs as a function

of their separation is neglected.

III. MONTE CARLO SIMULATION

The Monte Carlo chain of programs used in the simulation consists of an event generator, capable of following the development of the hadronic shower in the atmosphere and the muon transport code in the rock overburden, and a detector simulation package. We have used, as in all previous relevant analyses of muon events in MACRO [9,10], the HEMAS code [3] as an interaction model and shower simulator. Nuclear projectiles are handled by interfacing HEMAS with the "semi-superposition" model of the NUCLIB library [20]. The final relevant piece of simulation is the three-dimensional description of muon transport in the rock. A comparison of the performance of different transport codes, reported in Ref. [21], showed that the original package contained in the HEMAS code was too simplified, leading, for instance, to an underestimated muon survival probability at TeV energies. In order to verify possible systematics affecting the decoherence distribution, we repeated the Monte Carlo production, interfacing the more refined PROPMU code [19] to HEMAS. We have verified that, at least to first approximation, no changes in the shape of the decoherence function are noticeable between the two different simulation samples. For this reason, the sum of the two different Monte Carlo productions will be used in the following.

The map of Gran Sasso overburden as a function of direction and the description of its chemical composition are reported in Ref. [22]. The detector simulation is based on the CERN package GEANT [18]. The folding of simulated events with the detector simulation is performed according to a variance reduction method [23] to minimize statistical losses and reducing possible systematic errors.

We generated $3.6 \cdot 10^8$ primary interactions in the total energy range $3 \div 10^5$ TeV, assuming the "MACRO-fit" primary mass composition model [9,10], in which five mass groups (p, He,

CNO, Mg and Fe) are considered. Simulated data are produced with the same format as real data and are processed using the same analysis tools. After the application of the same cuts as for real data, a sample of about $7.0 \cdot 10^5$ muon pairs survived, corresponding to about 645 days of MACRO live time.

In Fig. 4 the comparison between the experimental and simulated decoherence curve inside the detector is shown. Curves are normalized to the peak of the dN/dD distribution. The remarkable consistency of the two curves demonstrates the HEMAS code capability to reproduce the observed data up to a maximum distance of 70 m. The bump in the experimental distribution around 40 m is due to the detector acceptance and is visible also in the simulated data, thus confirming the accuracy of our detector simulation. We also notice that, despite the application of cut C4, there is a non-negligible discrepancy between the experimental and simulated data in the first two bins of the distribution of $(34 \pm 2)\%$ and $(10 \pm 1)\%$, respectively. Such a discrepancy is not predicted by any model, since at short distances, apart from detector effects, the shape of decoherence distribution is dictated by the solid angle scaling: $dN/dD^2|_{D \to 0} \sim const.$, while the relevant properties of the interactions under investigation manifest themselves in the shape at large distances. The origin of this discrepancy will be discussed in detail in the last section of this paper, where other sources of contamination in the real data sample will be taken into account.

IV. UNFOLDING PROCEDURE

The agreement of the Monte Carlo and data shown in Fig. 4 proves that the simulation is consistent with observation and that the detector structure is well reproduced. A detector-independent analysis is required in order to subtract the geometric effects peculiar to MACRO, and allows a more direct comparison with other analyses and/or hadronic interaction models. This is accomplished by a correction method, built with the help of the

Monte Carlo simulation, to unfold the "true" decoherence function from the measured one in which geometrical containment and track reconstruction efficiencies are considered.

In the previous decoherence studies [7,8], the unfolding procedure was based on the evaluation of the detection efficiency for di-muon events generated by the Monte Carlo with a given angle and separation. Although this method is composition independent and allowed us to determine the detector acceptance with high statistical accuracy, it introduces systematic effects that have so far been neglected. In particular, in a multi-muon event it may happen that in a given projective view and in a particular geometrical configuration one muon track is "shadowed" by another. To avoid this effect, we adopt the following new unfolding method: the efficiency evaluation is performed considering the whole sample of events generated with their multiplicities. For a given bin of (D,θ,ϕ), where D is the muon pair separation and (θ,ϕ) is the arrival direction of the event, we calculate the ratio

$$\epsilon(D,\theta,\phi) = \frac{N^{in}(D,\theta,\phi)}{N^{out}(D,\theta,\phi)} \tag{4.1}$$

between the number of pairs surviving the selection cuts N^{in} and the number of pairs inserted in the detector simulator N^{out}. In principle, this choice of ϵ could be dependent on the primary mass composition model, since for a fixed distance D the efficiency (4.1) is dependent on the muon density and hence on its multiplicity, which in turn is correlated with the average atomic mass $\langle A \rangle$ of the primary. To check the systematic uncertainty related to this possibility, we evaluated the decoherence distributions obtained by unfolding the experimental data assuming the "heavy" and "light" composition models. Fig. 5 shows the relative comparison of the shape of the unfolding efficiencies as a function of pair separation, integrated in ($cos\theta, \phi$) after the normalization to the peak value. In the same plot we present the unfolding efficiency calculated with the method used in Ref. [7,8]. Considering the effect of the normalization, we observe that this method tends to overestimate the efficiencies in the low distance range, a consequence of the shadowing effect as explained in Section 2.

The unfolded decoherence is given by

$$\left(\frac{dN}{dD}\right)_{unf} = \sum_{(\theta,\phi)} \frac{N^{exp}(D,\theta,\phi)}{\epsilon(D,\theta,\phi)}, \tag{4.2}$$

where $N^{exp}(D,\theta,\phi)$ is the number of muon pairs detected with a separation D. In practice, we used 50 windows in $(cos\theta,\phi)$ space (5 and 10 equal intervals for $\cos\theta$ and ϕ, respectively).

The ability to evaluate the integral 4.2 for separate and independent windows constitutes a powerful check of the systematics related to the decoherence dependence on the variables $(cos\theta,\phi)$. Unfortunately this is not possible for r larger than 45 m, due to insufficient statistics. In that case the observables N^{in}, N^{out} and N^{exp} are integrated over $(cos\theta,\phi)$. We verified that the systematic error introduced by that choice is smaller than the present statistical error in that distance range.

Finally, unfolded experimental data obtained with the MACRO-fit model are directly compared with the Monte Carlo simulation (Fig. 6). The two curves are in good agreement although the disparity in the first bin of the distribution remains unresolved (see Section VI). The experimental values of the dN/dD distributions, normalized to the peak value, are reported in Table I.

V. UNCERTAINTIES OF THE HADRONIC INTERACTION MODEL

The present work, as are others from MACRO, is extensively based on the HEMAS code. This was explicitly designed to provide a fast tool for production of high energy muons (E_μ >500 GeV). However, as mentioned before, the interaction model of HEMAS is based on parametrizations of existing accelerator data and therefore is subject to the same risks of all this class of simulation codes. In particular, important correlations might be lost, or wrong, or the necessary extrapolations required by the specific kinematic regions of cosmic ray physics could yield unrealistic results. This remains a central problem of cosmic

ray physics. For this reason in the last few years general interest has grown in "physically inspired" simulations. These are based upon theoretical and phenomenological models like QCD and the Dual Parton Model [24], capable of properly constraining the predictions where data do not exist, without the introduction of a large number of free parameters. It is worthwhile to mention the attempt to merge the DPMJET model [25] into the shower simulation of HEMAS [26], and the interface of the CORSIKA shower code [27] with different models, like HDPM (the original interaction model of CORSIKA), VENUS [28], QGSJET [29], SIBYLL [30], and the afore mentioned DPMJET. A review of general results obtained using CORSIKA with those models has been provided by the Karlsruhe group [31]. A common feature of all these models is the more or less direct reference to the Regge-Gribov theories [32] for the soft contribution (low $P_\perp$). It must be stressed that such a phenomenological framework, by its nature, provides only predictions for the longitudinal properties of the interaction. The transverse structure leading to the specific $P_\perp$ distribution is not constrained by the theory, except for the higher $P_\perp$ phenomena, where perturbative QCD can be used (this is of small relevance in the primary energy region addressed by the MACRO data). Once again, the model builders have to be guided mostly by experimental data, introducing *a-priori* functional forms along with their additional required parameters. Some of the quoted models introduce proper recipes for the continuity between the soft and perturbative QCD regimes, and also specific nuclear phenomena like the Cronin effect mentioned above (see for instance [25]). In practice, the only possibility to evaluate a systematic uncertainty associated with the simulation model (at least those concerning the transverse structure of the showers) is to compare the predictions from all these models, HEMAS included. For this purpose, since the Karlsruhe report [31] did not address this point, we have performed test runs with some of the models interfaced to CORSIKA, to which PROPMU [19] has also been interfaced by us for muon transport in the rock overburden. A full simulation with all the other codes was outside our present capability, so we limited ourselves to comparisons at a

few fixed primary energies, and at fixed primary angles of 30° in zenith and 190° in azimuth. These correspond to an average rock overburden of $\sim$ 3200 hg/cm^2. In Tables II we show this comparison for a few representative average quantities for 3 different primary proton energies. We have considered the average depth of the first interaction X, $\langle P_\perp \rangle$ for pions coming from the first interaction, the average production slant height H_μ of muons surviving underground (the decay height of their parent mesons*.), the average distance of the muons from shower axis $\langle R \rangle$ and the average underground decoherence $\langle D \rangle$. Before discussing the results, it is important to remark that as far single interactions are concerned, all the models considered give a $P_\perp$ distribution following, with good approximation, the typical power law suggested by accelerator data. This is $\propto 1/(P_\perp + P_0)^\alpha$, although with somewhat different parameters for different models. Older models, like those predicting a simple exponential distribution for $P_\perp$, cannot reproduce the muon lateral distribution observed in MACRO data [7].

In the energy range of 100-1000 TeV, to which most of MACRO data belong, the resulting differences in the average muon separation do not exceed 20%. These discrepancies seem to reduce at higher energy, while they appear much larger at few tens of TeV. DPMJET is probably the only model predicting a higher average separation than HEMAS. A precise analysis of the reasons leading to the differences among models is complicated. However, we note that HEMAS gives in general higher values of average $P_\perp$ than the other models. The only exception is indeed DPMJET, which, as mentioned before, pays particular attention to the reproduction of nuclear effects affecting the transverse momentum, as measured in heavy ion experiments [33]. On the other hand, the effect of this large $P_\perp$ on the lateral distribution of muons is moderated in HEMAS by a deeper shower penetration (the inelastic

*CORSIKA does not allow direct access to the production height of parent mesons, which would be more interesting for our purposes

cross section is based on Ref. [34]); in general HEMAS exhibits a somewhat smaller height of meson production.

Similar features in the comparison of models are also obtained for nuclear projectiles. It is therefore conceivable that, for the same primary spectrum and composition, not all the models considered could reproduce the MACRO decoherence curve. Thus the best fit for spectrum and composition as derived from the analysis of muon multiplicity distribution in MACRO will also probably differ according to the model.

At least in part, the decoherence analysis can disentangle different ranges of longitudinal components of the interaction from the transverse ones, if this is performed in different zenith angle and rock depth windows. In fact, larger zenith angles correspond (on average) to larger muon production slant heights. This is a geometrical effect due to the greater distance from the primary interaction point to the detector for large zenith angle and consequently to the greater spreading of the muon bundle before reaching the apparatus. Larger rock depths select higher energy muons and consequently higher average energy of their parent mesons. The average separation decreases with the rock depth since, qualitatively, the longitudinal momentum $\langle P_{\parallel} \rangle$ increases linearly with energy while $\langle P_{\perp} \rangle$ increases only logarithmically. The overall result of increasing rock depth is the production of final states in a narrower forward cone, decreasing the muon pair average separation observed at the detector level.

In Fig. 7 and 8 the unfolded decoherence function is compared to the HEMAS prediction for different zenith and rock depth intervals. In Table III, the average separation $\langle D \rangle$ is reported as a function of $cos\theta$ and rock depth for fixed rock depth and zenith, respectively. In the same table we report the average values of slant height of first interaction $\langle X \rangle$, muon production slant height $\langle H_{\mu} \rangle$, energy $\langle E_p \rangle$ and transverse momentum $\langle P_{\perp} \rangle$ of the parent mesons, as obtained from the HEMAS Monte Carlo in the same windows.

The agreement between the results and the Monte Carlo in separate variable intervals reinforces our confidence in the capability of HEMAS to reproduce the significant features

of shower development. This also allows us to exclude the existence of significant systematic errors related to this analysis.

VI. THE CONTRIBUTION OF THE $\mu^{\pm} + N \rightarrow \mu^{\pm} + N + \mu^{+} + \mu^{-}$ PROCESS AT SMALL DISTANCES

The capability of the MACRO detector to resolve very closely spaced tracks permits the extension of the decoherence analysis to a distance region hardly studied in the past. The mismatch between experimental and simulated data in this region ($D \leq 160$ cm) has been emphasized earlier in our discussion. In Section 2 a solution was attempted, permitting us to discard, with high efficiency, those tracks originating from secondary particle production. However, Fig. 4 and Fig. 6 show that other sources of contamination in the first bin of the decoherence function are responsible for the discrepancy.

The process of muon pair production by muons in the rock, $\mu^{\pm} + N \rightarrow \mu^{\pm} + N + \mu^{+} + \mu^{-}$, is a natural candidate. As pointed out in [16], at the typical muon energy involved in underground analyses ($E_{\mu} \sim 1$ TeV) and for very large energy transfer, the cross section for this process is non-negligible with respect to $e^{+}e^{-}$ pair production. An analytic expression for the muon pair production cross section is given in [16,35]. In order to test the hypothesis, such a cross section has been included in the muon transport code PROPMU. Assuming a muon flux with energy spectrum $E^{-3.7}$ and minimum muon energy $E_{\mu}^{min} = 1.2$ TeV at the surface, and considering the actual mountain profile, we generated a sample of 10^7 muons corresponding to 3666 h of live time. About $\sim 3.0 \cdot 10^6$ muons survived to the MACRO level, 5360 of which were generated by muon pair production processes. The average separation of these muon pairs is (128 ± 1) cm, and their average residual energies are (657 ± 14) GeV and (145 ± 3) GeV, respectively, for the main muon and the secondary muon samples. We propagated the muons surviving to the MACRO level through the GEANT simulation and

we applied the same cuts specified in Section 2. Finally, the number of events was normalized to the live time of real data.

In Table IV we report the number of weighted muon pairs in the first bins of the experimental and simulated decoherence distributions (in the form dN/dD). The effect of standard cuts, of cut C4, and of the subtraction of the muon pair production process are shown in order. In each case, we indicated in percentage the bin populations with respect to the peak of the distribution and the discrepancy with respect to the Monte Carlo predictions.

In Fig. 9 we compare the simulated decoherence curve with the data corrected for the muon pair production effect. Despite the approximation introduced in our test, it seems that the proposed muon pair production process can account for most of the observed discrepancy in the low distance range. This is also shown in the inset of Fig. 9 where the distribution of relative distance for the muon pairs in excess of the data (after subtraction of HEMAS prediction) is compared to the expectation from simulated muon pair production.

An excess at small pair separation is also predicted in exotic processes, like multi-W production by AGN ν's, as suggested in [36]. However, according to this reference, muons from W$\rightarrow\mu+\nu$ decay have an average energy of $\simeq$80 TeV. These muons would survive underground with a residual energy much higher than that of standard muons, producing local catastrophic interaction in the detector, making difficult their identification as a pair. On the contrary, the explanation proposed here is based on a pure QED process that does not require any additional physics.

VII. DISCUSSION AND CONCLUSIONS

We have obtained an improved experimental underground decoherence function using high energy muons ($E_\mu > 1.3\ TeV$) up to a maximum distance of about 70 m. It is hard to conceive in the near future a large area underground experiment capable of improving the

sensitivity reached in this decoherence study.

A new unfolding of the experimental distribution confirms the results obtained with the analysis within the detector.

The ability to resolve closely spaced muon tracks allows an investigation of the decoherence function at small separations. Apart from the negligible contamination of hadroproduction by muons (which will be the subject of a future work), we found that a relevant contribution is made by the process $\mu^{\pm} + N \rightarrow \mu^{\pm} + N + \mu^{+} + \mu^{-}$. The inclusion of this interaction in the simulation reproduces, in both a qualitative and a quantitative way, the experimental data.

The agreement of the overall distribution shape for experimental and simulated data from HEMAS is excellent. The possible excess at high muon separations suggested in the previous, preliminary, analyses [7,8] was due to an imperfect unfolding procedure, and is now excluded. These results both in the integrated distribution and in those from separate intervals of zenith and rock depth, shows that HEMAS gives a reasonable account of the cascade development and that it is not necessary to introduce any anomalous $P_{\perp}$ production in the Monte Carlo to reproduce these data. However, the other interaction models considered for comparison, while reproducing similar behaviour, in general give different combinations of transverse momentum and production height. Discrimination among the different models may be possible only after a complete simulation and analysis of MACRO data with each of the codes. Therefore the present work, representing a final data reduction and analysis, provides a valuable benchmark for future analysis dedicated to the investigation of the properties of high energy interactions and to the evaluation of different shower models in the primary energy region spanning from a few tens to a few thousands TeV/nucleon. The detector independent analysis described here will make this task easier.

REFERENCES

[1] T.K. Gaisser, *Proc. Vulcano Workshop 1992 "Frontier Objects in Astrophys. and Particle Phys."*, **40**, 433 (1993).

[2] P. Sokolsky, *Introduction to Ultra High Energy Cosmic Ray Physics*, Addison & Wesley Publishing Co. (1988), p. 131.

[3] C. Forti et al., Phys. Rev. **D42** 3668 (1990).

[4] H.E. Bergeson et al., Phys. Rev. Lett. **35** 1681 (1975).

[5] G. Battistoni et al, LNGS-95-09 (1995); G. Battistoni et al, in *Proceedings of the XXIV Int. Cosmic Ray Conf.*, Roma, Italy, 1995, ed. N. Iucci et al., Arti Grafiche Editoriali, Urbino, (1995), Vol. 1, p. 508.

[6] MACRO Collaboration, S.P. Ahlen et al., Nucl. Instr. Meth. **A324** 337 (1993).

[7] MACRO Collaboration, S.P. Ahlen et al., Phys. Rev. **D46** 4836 (1992).

[8] MACRO Collaboration, S.P. Ahlen et al., *Proceedings of the XXIII Int. Cosmic Ray Conf.*, Calgary, Canada, 1993, ed. R.B. Hicks et al., World Scientific, Singapore, (1994), Vol. 2, p. 93.

[9] MACRO Collaboration, M. Ambrosio et al., Phys. Rev. **D56** 1407 (1997).

[10] MACRO Collaboration, M. Ambrosio et al., Phys. Rev. **D56** 1418 (1997).

[11] G. Auriemma et al., *Proceedings of the XXI Int. Cosmic Ray Conf.*, Adelaide, Australia, 1989, ed. R.J. Protheroe, Graphic Services, Northfield, Australia, (1990), Vol. 9, p. 362.

[12] J.W. Cronin et al., Phys. Rev. **D11** 3105 (1975).

[13] M. Bardadin-Otwinowoka et al., *Proceedings of the Vienna Conference on Elementary Particles*, Vol. 1, 628 (1963).

[14] SOUDAN2 Collaboration, S.M.S. Kasahara et al., Phys. Rev. **D55** 5282 (1997).

[15] MACRO Collaboration, M. Ambrosio et al., *Proceedings of the XXV Int. Cosmic Ray Conf.*, Durban, South Africa, 1997, ed. M.S. Potgieter et al., Wesprint, Potchefstroom, (1997), Vol. 6, p. 357.

[16] V.A. Kudryavtsev and O.G. Ryazhskaya, INFN-AE-97-08 (1997); V.A. Kudryavtsev and O.G. Ryazhskaya, in *Proceedings of the XXV Int. Cosmic Ray Conf.*, (1997), Vol. 6, p. 405.

[17] A. Fassó et al., An update about FLUKA, Proc. 2nd workshop on Simulating Accelerator Radiation Environment, SARE-2, CERN-Geneva, 9-11, October, 1995.

[18] R. Brun et al., CERN GEANT3 User's guide, DD/EE/84-1 (1992).

[19] P. Lipari and T. Stanev, Phys. Rev **D44** 3543 (1991).

[20] J. Engels et al., Phys. Rev. D **46**, 5013 (1992).

[21] G. Battistoni et al., Nucl. Instr. Meth. **A394** 136 (1997).

[22] MACRO Collaboration, M. Ambrosio et al., Phys. Rev. **D52** 3793 (1995).

[23] G. Battistoni et al., Astroparticle Phys. **7** 101 (1997).

[24] A. Capella et al., Phys. Rep. **236** 225 (1994).

[25] J. Ranft, Phys. Rev. **D51** 64 (1995).

[26] G. Battistoni et al., Astropart. Phys. **3** 157 (1995).

[27] J.N. Capdevielle et al., *the Karlsruhe extensive air shower simulation code CORSIKA*, KFK Report 4998 (1992).

[28] K. Werner, Phys. Rep. **232** 87 (1993).

[29] N.N. Kalmikov et al, Physics of Atomic Nuclei **58** 1728 (1995).

[30] R.S. Fletcher et al., Phys. Rev. **D50** 5710 (1994).

[31] J. Knapp, D. Heck and G. Schatz, *Comparison of hadronic interaction models used in Air shower simulations and their influence on shower development and observables*, Karlsruhe report FZKA 5828 (1996).

[32] V.N. Gribov, Sov. Phys. JETP **26** 414 (1968); V.N. Gribov and A.A. Migdal, Sov. J. Nucl. Phys. **8** 583 (1969); see also M. Baker and K.A. Ter-Martirosyan *Gribov's Reggeon calculus: its physical basis and implication*, Phys. Rep. **28C** 1 (1976).

[33] See the review of H.R Schmidt and J. Schukraft, GSI–preprint GSI-92-19 (1992).

[34] L. Durand and H. Pi, Phys. Rev. Lett. **58** 303 (1987).

[35] S.R. Kelner, Sov. J. Nucl. Phys. **5** 778 (1967).

[36] D.A.Morris and A.Ringwald, Astropart. Phys. **2** 43 (1994).

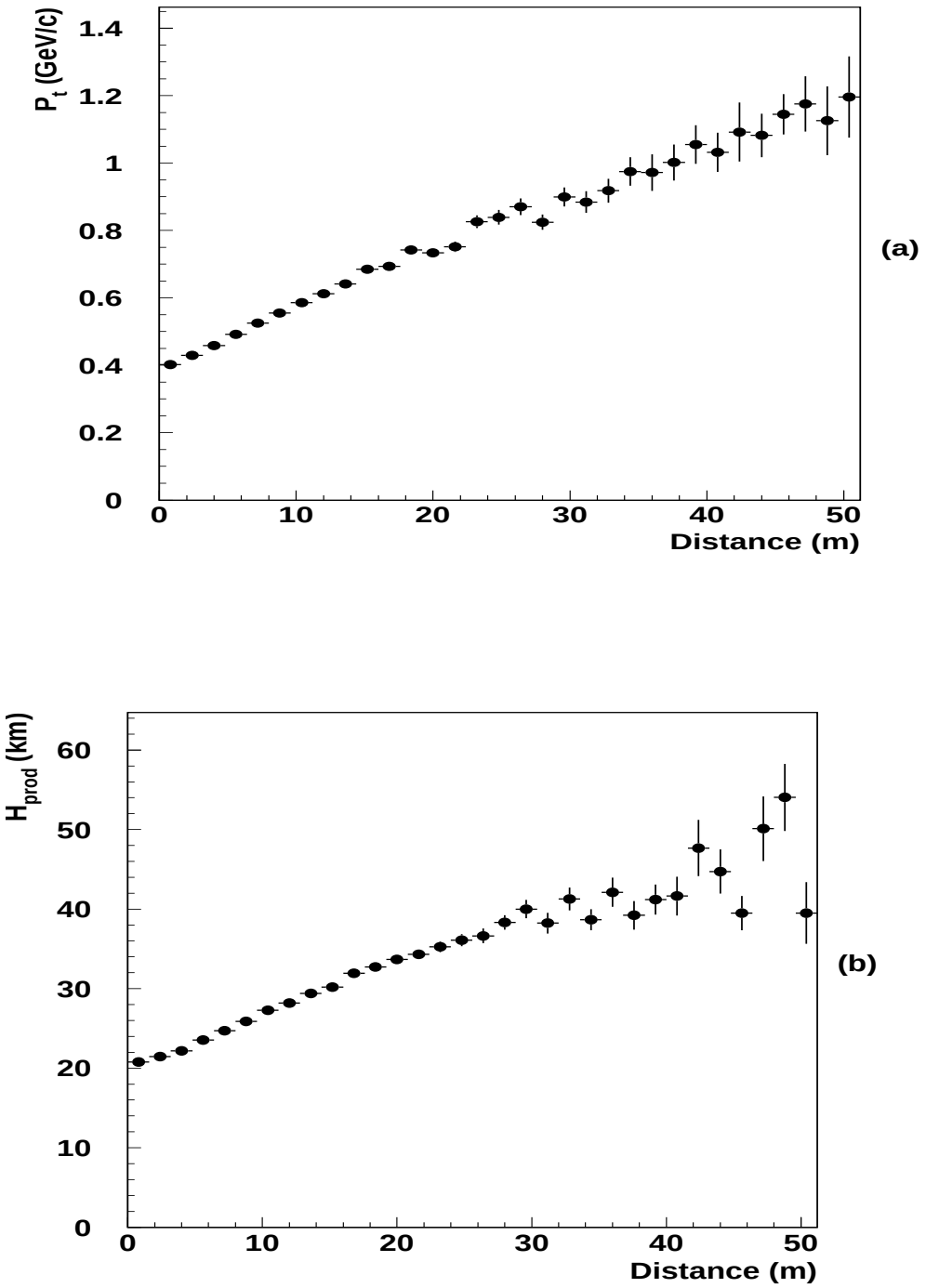

FIG. 1. *Average separation of underground muon pairs at Gran Sasso depth, as a function of* $\langle P_\perp \rangle$ *of the parent mesons (a) and of the slant height in the atmosphere (b). The results are obtained with the HEMAS Monte Carlo.*

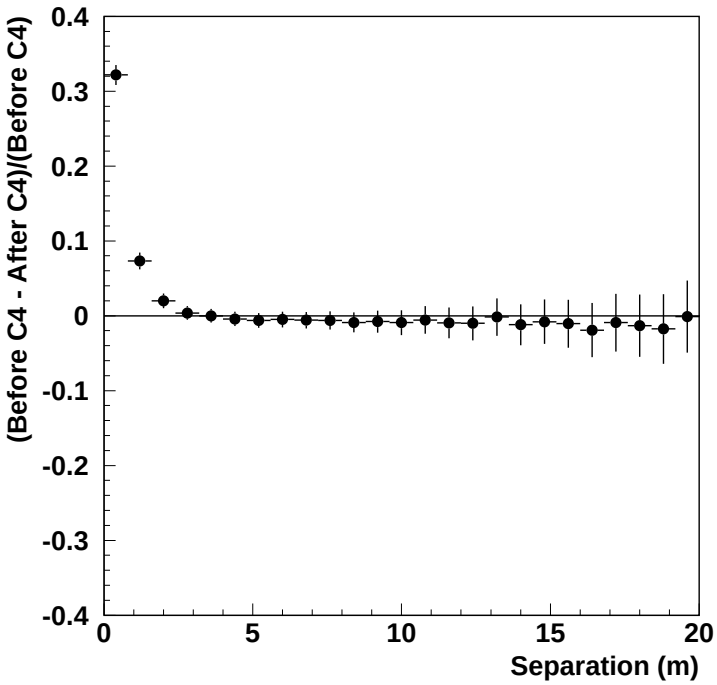

FIG. 2. *The change in the experimental decoherence function induced by cut C4. The data indicate the fractional deviation between the experimental decoherence function before and after the application of the cut.*

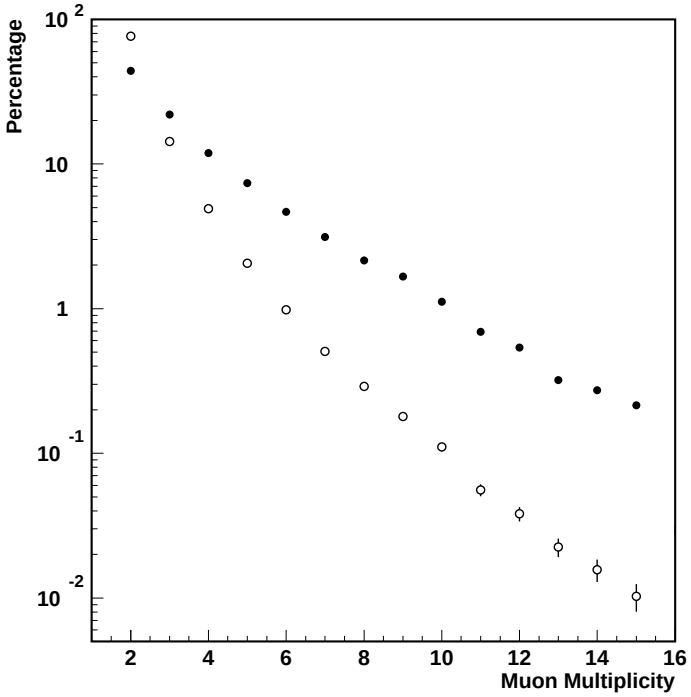

FIG. 3. *Percentage of reconstructed real events (white points) and unambiguously associated muon pairs (black points) as a function of event multiplicity.*

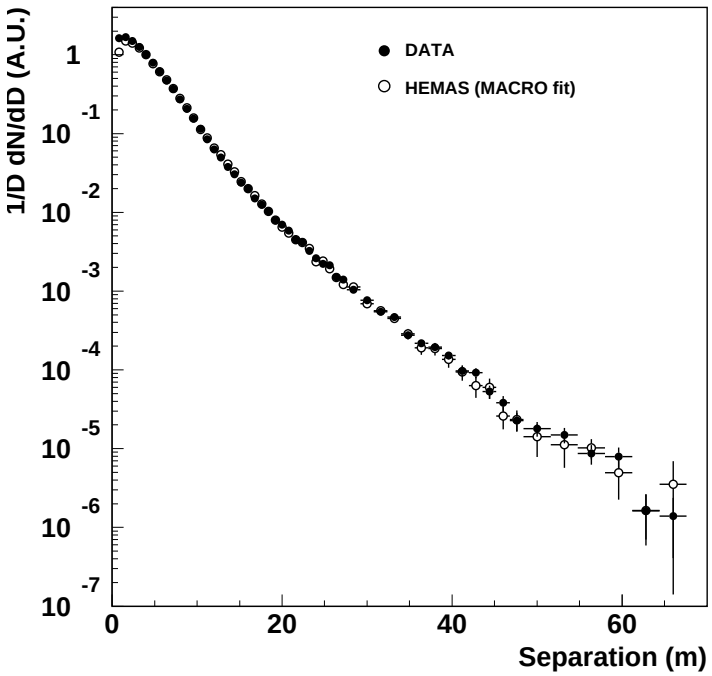

FIG. 4. *Experimental (black points) and simulated (white points) decoherence function, normalized to the peak of the dN/dD distribution. The second to last points of the two distributions coincide.*

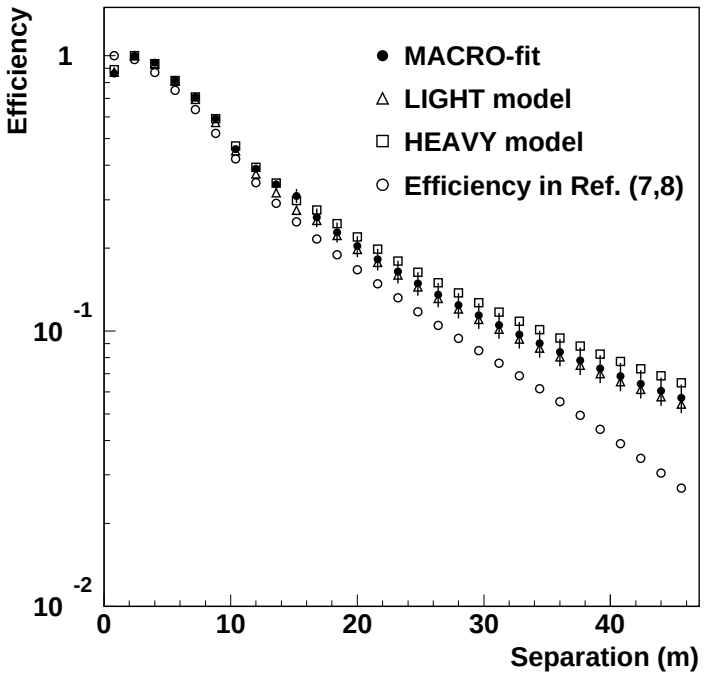

FIG. 5. *Comparison of the unfolding efficiencies as a function of pair separation for different composition models. The curves are normalized to the peak value. For comparison, we include the efficiency evaluated with the method used in previous analyses (white points).*

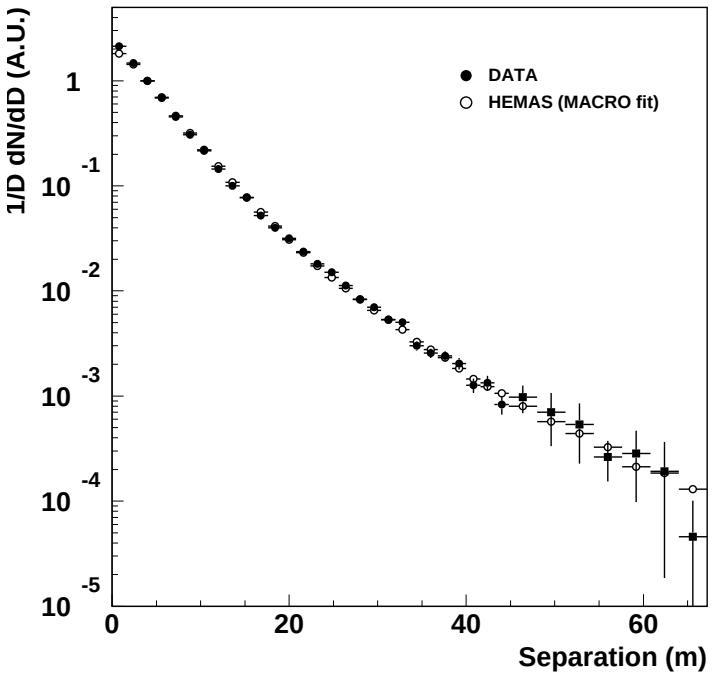

FIG. 6. *Unfolded experimental decoherence distribution compared with the infinite-detector Monte Carlo expectation, computed with the HEMAS interaction code and the MACRO-fit primary composition model. Black squares represent data above 45 m (integral form unfolding).*

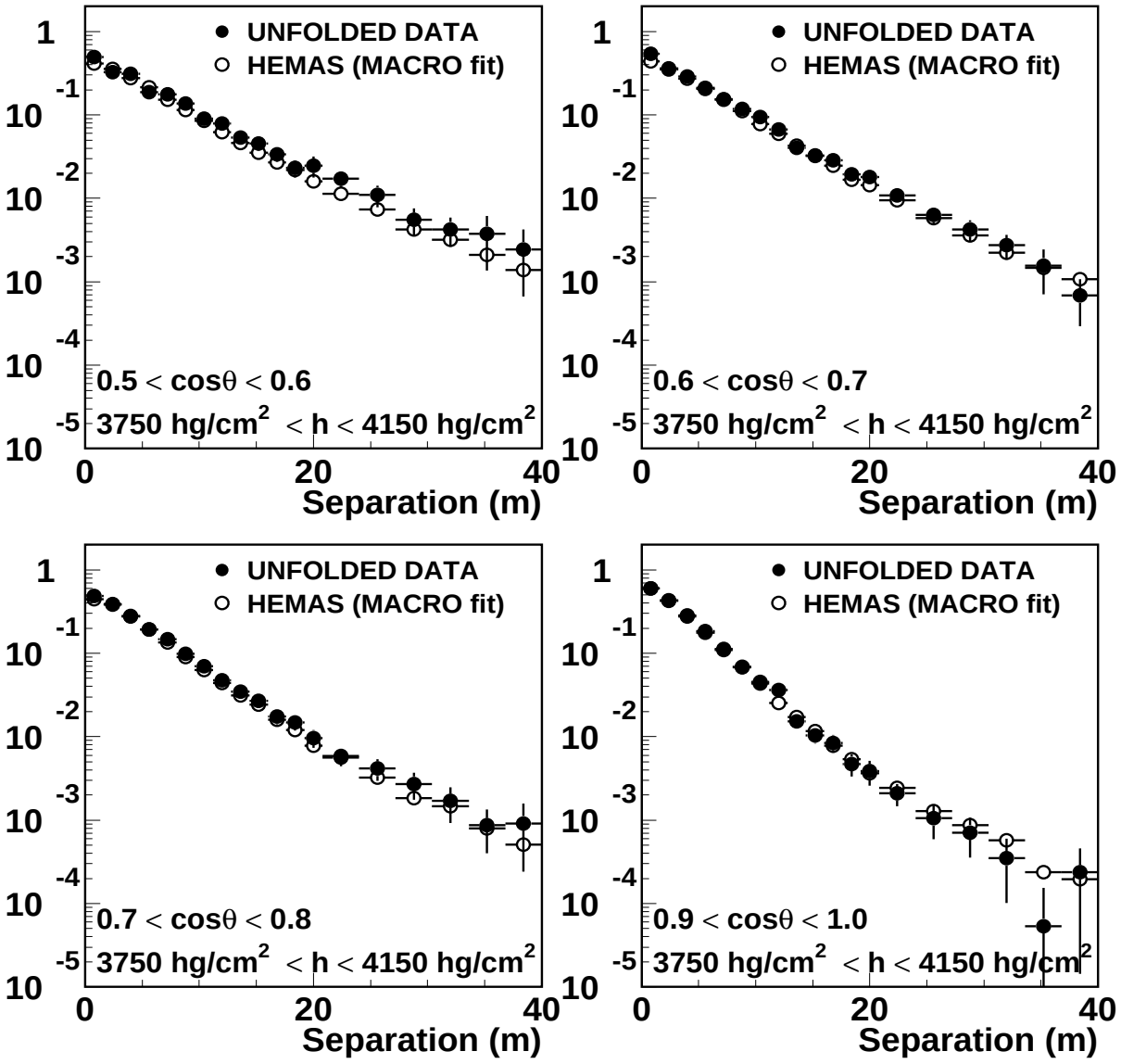

FIG. 7. *Unfolded decoherence functions compared with Monte Carlo simulations for different cosθ windows. The vertical scale is in arbitrary units.*

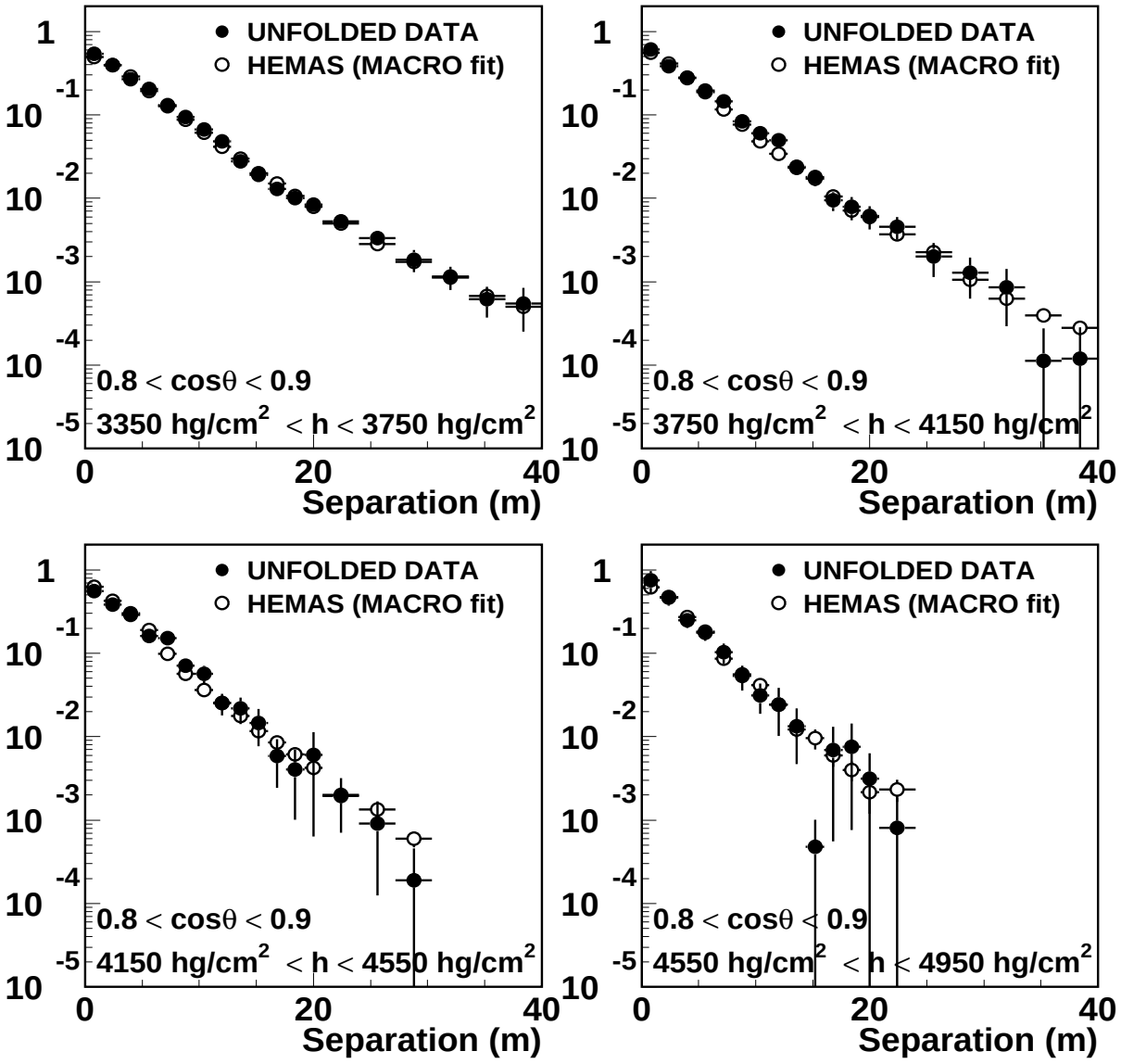

FIG. 8. *Unfolded decoherence functions compared with Monte Carlo simulations for different rock depth windows.*

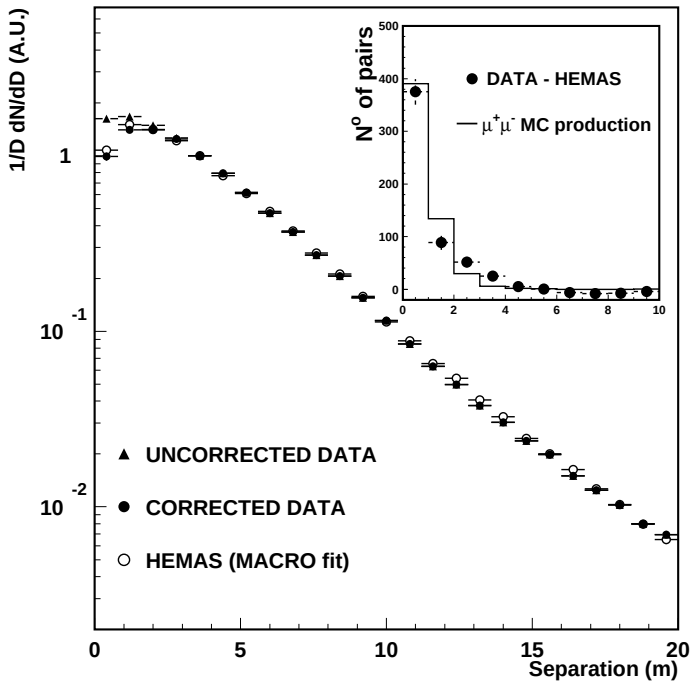

FIG. 9. *The low distance region of the experimental decoherence function, before and after the subtraction of the secondary muon sample, and comparison with the Monte Carlo simulation. The inset shows the distribution of relative distance for muon pairs in excess of the data after the subtraction of the HEMAS prediction, as compared to the expectation from simulated muon pair production in the rock.*

TABLES

D (cm)	$\frac{dN}{dD}$	Error
80	0.4254	$0.1034\ 10^{-1}$
240	0.8855	$0.1591\ 10^{-1}$
400	1.0000	$0.1738\ 10^{-1}$
560	0.9591	$0.1719\ 10^{-1}$
720	0.8148	$0.1554\ 10^{-1}$
880	0.6730	$0.1419\ 10^{-1}$
1040	0.5595	$0.1350\ 10^{-1}$
1200	0.4341	$0.1216\ 10^{-1}$
1360	0.3410	$0.1118\ 10^{-1}$
1520	0.2939	$0.1144\ 10^{-1}$
1680	0.2198	$0.4950\ 10^{-2}$
1840	0.1828	$0.4626\ 10^{-2}$
2000	0.1578	$0.4476\ 10^{-2}$
2160	0.1283	$0.4134\ 10^{-2}$
2320	0.1047	$0.3906\ 10^{-2}$
2480	$0.9348\ 10^{-1}$	$0.3881\ 10^{-2}$
2640	$0.7438\ 10^{-1}$	$0.3599\ 10^{-2}$
2800	$0.5847\ 10^{-1}$	$0.3211\ 10^{-2}$
2960	$0.5168\ 10^{-1}$	$0.3238\ 10^{-2}$
3120	$0.4173\ 10^{-1}$	$0.2994\ 10^{-2}$
3280	$0.4113\ 10^{-1}$	$0.3125\ 10^{-2}$
3440	$0.2582\ 10^{-1}$	$0.2585\ 10^{-2}$
3600	$0.2315\ 10^{-1}$	$0.2444\ 10^{-2}$
3760	$0.2260\ 10^{-1}$	$0.2522\ 10^{-2}$

3920	$0.2004\ 10^{-1}$	$0.2501\ 10^{-2}$
4080	$0.1289\ 10^{-1}$	$0.2023\ 10^{-2}$
4240	$0.1419\ 10^{-1}$	$0.2319\ 10^{-2}$
4400	$0.9105\ 10^{-2}$	$0.1775\ 10^{-2}$
4560	$0.6776\ 10^{-2}$	$0.1597\ 10^{-2}$
4720	$0.3080\ 10^{-2}$	$0.1035\ 10^{-2}$
4880	$0.2990\ 10^{-2}$	$0.1121\ 10^{-2}$
4640	$0.1128\ 10^{-1}$	$0.3340\ 10^{-2}$
4960	$0.8697\ 10^{-2}$	$0.4549\ 10^{-2}$
5280	$0.7108\ 10^{-2}$	$0.4098\ 10^{-2}$
5600	$0.3689\ 10^{-2}$	$0.1534\ 10^{-2}$
5920	$0.4190\ 10^{-2}$	$0.2742\ 10^{-2}$
6240	$0.2991\ 10^{-2}$	$0.2703\ 10^{-2}$
6560	$0.7539\ 10^{-3}$	$0.9004\ 10^{-3}$

TABLE I. *Tabulation of the the unfolded decoherence distribution as measured by MACRO. The data points are normalized to the point of maximum.*

p–Air, 20 TeV

Code	$\langle X_{first} \rangle$ (g/cm^2)	$\langle P_\perp \rangle$ $\pi^\pm$ (GeV/c)	$\langle H_\mu \rangle$ (km)	$\langle R \rangle$ (m)	$\langle D \rangle$ (m)
HEMAS	51.4	0.40	24.1	7.9	12.7
CORSIKA/DPMJET	44.4	0.42	25.6	10.1	13.9
CORSIKA/QGSJET	45.7	0.39	24.3	7.3	10.0
CORSIKA/VENUS	48.3	0.35	24.5	7.4	8.3
CORSIKA/SIBYLL	50.9	0.37	23.5	7.2	11.5

p–Air, 200 TeV

Code	$\langle X_{first} \rangle$ (g/cm^2)	$\langle P_\perp \rangle$ $\pi^\pm$ (GeV/c)	$\langle H_\mu \rangle$ (km)	$\langle R \rangle$ (m)	$\langle D \rangle$ (m)
HEMAS	56.1	0.44	20.6	5.3	8.0
CORSIKA/DPMJET	53.9	0.43	21.7	6.2	8.8
CORSIKA/QGSJET	52.8	0.41	21.4	5.5	7.8
CORSIKA/VENUS	60.2	0.36	20.9	5.3	7.5
CORSIKA/SIBYLL	55.2	0.41	20.2	5.2	7.3

p–Air, 2000 TeV

Code	$\langle X_{first} \rangle$ (g/cm^2)	$\langle P_\perp \rangle$ $\pi^\pm$ (GeV/c)	$\langle H_\mu \rangle$ (km)	$\langle R \rangle$ (m)	$\langle D \rangle$ (m)
HEMAS	63.0	0.50	16.3	4.1	6.0
CORSIKA/DPMJET	60.0	0.42	18.5	4.9	6.4
CORSIKA/QGSJET	63.1	0.44	17.7	4.2	5.6
CORSIKA/VENUS	66.7	0.36	16.8	4.1	5.3

CORSIKA/SIBYLL	60.3	0.44	17.0	4.4	5.6

TABLE II. *Comparison of a few relevant quantities concerning the lateral distribution of underground muons at the depth of 3200 hg/cm^2, from proton primaries at 20, 200 and 2000 TeV, 30° zenith angle. The statistical errors are smaller than the last reported digit.*

3750<h<4150 (hg/cm^2)

		.5<cosθ<.6	.6<cosθ<.7	.7<cosθ<.8	.8<cosθ<.9	.9<cosθ<1.
EXP	$\langle D \rangle$ (m)	13.2 ± 2.3	11.4 ± 2.2	10.3 ± 2.2	8.5 ± 1.9	7.5 ± 1.9
	$\langle D \rangle$ (m)	12.8 ± 1.4	12.0 ± 1.3	10.1 ± 1.2	8.8 ± 1.2	7.8 ± 1.1
	$\langle X \rangle$ (km)	65.9 ± 0.2	57.0 ± 0.2	51.2 ± 0.3	42.5 ± 0.4	37.0 ± 0.5
MC	$\langle H_\mu \rangle$ (km)	41.6 ± 0.3	34.3 ± 0.3	28.1 ± 0.3	23.8 ± 0.3	20.4 ± 0.3
	$\langle E_p \rangle$ (TeV)	4.1 ± 0.2	4.0 ± 0.2	4.0 ± 02	3.9 ± 0.1	3.9 ± 0.2
	$\langle P_\perp \rangle$ (GeV/c)	0.56 ± 0.01	0.59 ± 0.01	0.57 ± 0.01	0.57 ± 0.02	0.57 ± 0.01

(a)

0.8<cosθ<0.9

		3350<h<3750 (hg/cm^2)	3750<h<4150 (hg/cm^2)	4150<h<4550 (hg/cm^2)	4550<h<4950 (hg/cm^2)
EXP	$\langle D \rangle$ (m)	9.4 ± 2.1	8.5 ± 1.9	7.3 ± 1.6	6.2 ± 1.6
	$\langle D \rangle$ (m)	9.7 ± 3.4	8.8 ± 1.2	7.7 ± 1.1	7.1 ± 1.1
	$\langle X \rangle$ (km)	42.7 ± 0.4	$42.5 \pm .4$	45.9 ± 0.3	43.76 ± 0.3
MC	$\langle H_\mu \rangle$ (km)	23.7 ± 0.3	23.8 ± 0.3	24.6 ± 0.3	25.1 ± 0.5
	$\langle E_p \rangle$ (TeV)	3.6 ± 0.1	3.9 ± 0.1	4.4 ± 0.1	4.8 ± 0.02
	$\langle P_\perp \rangle$ (GeV/c)	0.56 ± 0.02	0.57 ± 0.02	0.58 ± 0.02	0.58 ± 0.02

(b)

TABLE III. *Average separation between muon pairs $\langle D \rangle$ (in m) as a function of cosθ (a) and rock depth (b). In each table the experimental data are compared to the expectations from the HEMAS Monte Carlo. For the same simulations, other averages of relevant quantities are reported.*

	0–80 cm	80–160 cm	160–240 cm	240–320 cm	320–400 cm (max)
Exp. Data	5528	12491	17569	20514	20816
MC Data	5154	21417	33573	40367	42679
Discrepancy after normalization	(55±2)%	(16±2)%	(6±1)%	(4±1)%	
Exp. Data + C4	3612	11128	16535	19597	19977
MC Data + C4	4848	20346	31932	38425	40660
Discrepancy after normalization	(34±2)%	(10±2)%	(6±2)%	(4±2)%	
Exp. Data + C4 + μ pair subtraction	2193	9264	15462	19190	19842
MC Data + C4	4848	20346	31932	38425	40660
Discrepancy after normalization	(8±7)%	(7±3)%	(0±2)%	(2±2)%	

TABLE IV. *Number of weighted muon pairs in the first few bins of the experimental and simulated decoherence distributions. The discrepancy is the percentage difference between experimental and Monte Carlo values, normalized to the distribution maximum (last column).*